

Improving the Utility of Differentially Private Clustering through Dynamical Processing

Junyoung Byun^a, Yujin Choi^b, Jaewook Lee^{b,*}

^a*Chung-Ang University, 84, Heukseok-ro, Seoul, 06974, Republic of Korea*

^b*Seoul National University, 1, Gwanak-ro, Seoul, 08826, Republic of Korea*

Abstract

This study aims to alleviate the trade-off between utility and privacy of differentially private clustering. Existing works focus on simple methods, which show poor performance for non-convex clusters. To fit complex cluster distributions, we propose sophisticated dynamical processing inspired by Morse theory, with which we hierarchically connect the Gaussian sub-clusters obtained through existing methods. Our theoretical results imply that the proposed dynamical processing introduces little to no additional privacy loss. Experiments show that our framework can improve the clustering performance of existing methods at the same privacy level.

Keywords:

Clustering, Differential privacy, Dynamical Processing, Morse Theory

*Corresponding author at: Seoul National University, 1, Gwanak-ro, Seoul, 08826, Republic of Korea

E-mail addresses: junyoungb@cau.ac.kr (J. Byun), uznhigh@snu.ac.kr (Y. Choi), jae-wook@snu.ac.kr (J. Lee)

1. Introduction

Machine learning algorithms can inadvertently expose sensitive information about individuals used for training. Differential privacy (DP) offers a mathematical guarantee to prevent the leakage of personal information from algorithm outputs, although it often comes at the cost of reduced algorithm performance. Consequently, research in differentially private machine learning focuses on maintaining algorithm performance while ensuring privacy.

Clustering is widely used in applications like recommendation systems, marketing, and fraud detection, where protecting customer information is crucial [1, 2]. However, differentially private clustering has received less attention compared to supervised learning. Existing studies primarily address simple methods such as k-means clustering [3, 4] and mixtures of Gaussians (MoGs) [5, 6, 7], which struggle to represent complex, nonconvex cluster structures.

Inspired by Morse theory from differential topology, Morse clustering remains an active area of research [8, 9]. [10] applied Morse theory to enhance the performance of non-private support vector-based clustering algorithms. However, applying DP to their method is challenging because calculating the kernel function during inference requires support vectors from the training data.

This study addresses these limitations by applying Morse theory to enhance differentially private clustering algorithms. Our method leverages MoG models, which do not require training data once the density function is estimated. From the MoG density function obtained through differentially private clustering, we build an associated dynamical system and construct

a weighted graph to connect Gaussian sub-clusters, effectively representing complex clusters through the merging of sub-clusters.

Theoretical results demonstrate that the proposed dynamical processing is DP-friendly, introducing minimal additional privacy loss beyond existing methods. Furthermore, our method is inductive and capable of achieving any desired number of clusters.

2. Related Works

Recent research has focused on improving the sample-and-aggregate framework. [11] introduced an enhanced framework for well-separated datasets, offering better DP guarantees and sample complexity bounds. [12] applied a sample-and-aggregate framework to MoG models. [13] and [14] investigated differentially private DBSCAN algorithms. Recently, [4] proposed a genetic algorithm-based privacy budget allocation strategy in differentially private k-means algorithm.

3. Differential Privacy

DP [15] defines privacy by limiting how much a mechanism's output can change with alterations in the dataset.

Definition 3.1. (Differential privacy) A randomized mechanism \mathcal{M} is (ϵ, δ) -differentially private if for any set of possible outputs $\mathcal{S} \subseteq \text{Range}(\mathcal{M})$ and two neighboring datasets $D, D' \in \mathcal{D}$ which differ in exactly one data sample:

$$\Pr[\mathcal{M}(D) \in \mathcal{S}] \leq e^\epsilon \Pr[\mathcal{M}(D') \in \mathcal{S}] + \delta. \quad (1)$$

When $\delta = 0$, the mechanism \mathcal{M} is called ϵ -differentially private.

In this definition, ϵ is called the *privacy budget*, indicating that privacy degrades as ϵ increases. A well-known result of DP is composition, which states that privacy degrades with multiple data accesses. While the most widely recognized composition method is advanced composition [15], this study utilizes a variant of DP called zero-concentrated DP (zCDP) [16], which provides a tighter analysis of privacy loss. Below we introduce some properties of zCDP relevant to this paper.

Remark 3.2. (Proposition 1.3 [16]) If \mathcal{M} satisfies ρ -zCDP, then \mathcal{M} satisfies $(\rho + 2\sqrt{\rho \log(1/\delta)}, \delta)$ -DP for any $\delta > 0$.

Remark 3.3. (Proposition 1.4 [16]) If \mathcal{M} satisfies ϵ -DP, then \mathcal{M} satisfies $\frac{1}{2}\epsilon^2$ -zCDP.

Remark 3.4. (Proposition 1.6 [16]) Let function $f : \mathcal{X}^n \rightarrow \mathbb{R}$ has a sensitivity Δ . Then on input x , releasing a sample from $\mathcal{N}(f(x), \sigma^2)$ satisfies $(\Delta^2/2\sigma^2)$ -zCDP.

Remark 3.5. (Lemma 1.8 [16]) Let randomized mechanisms \mathcal{M}_1 and \mathcal{M}_2 satisfy ρ_1 -zCDP and ρ_2 -zCDP, respectively. Then the mapping $\mathcal{M}_{1,2} = (\mathcal{M}_1, \mathcal{M}_2)$ satisfies $(\rho_1 + \rho_2)$ -zCDP.

Two important properties of DP, post-processing and parallel composition, allow for controlling privacy loss. Post-processing states that any processing that does not access the data does not increase the privacy loss.

Remark 3.6. (Post-Processing) Let the randomized mechanism \mathcal{M} be (ϵ, δ) -differentially private. Then, for any data-independent randomized mapping f , $f \circ \mathcal{M}$ is also (ϵ, δ) -differentially private.

When the data is partitioned, we can exploit parallel composition.

Remark 3.7. (Parallel Composition) Let the dataset D be partitioned by disjoint subset D_i for $i = 1, 2, \dots, n$ and let \mathcal{M}_i is ϵ_i - differentially private mechanism which takes D_i as input. Then, releasing all of the results $\mathcal{M}_1, \mathcal{M}_2, \dots, \mathcal{M}_n$ is $\max_i \epsilon_i$ -differentially private.

4. Morse Theory from a Dynamical System Perspective

4.1. Morse theory

Let $\{\mathbf{x}_i\} \subset \mathcal{X}$ be a given dataset of N points, with $\mathcal{X} := \mathbb{R}^D$, the data space. Given a smooth real-valued function $f : \mathcal{X} \rightarrow \mathbb{R}$ mapping each point to its height, the inverse image of a point $a \in \mathbb{R}$, called a level set, can be decomposed into several separate connected components C_i , $i = 1, \dots, m$, i.e.,

$$\mathcal{X}_a := f^{-1}(-\infty, a] = \{\mathbf{x} \in \mathcal{X} : f(\mathbf{x}) \leq a\} = C_1 \cup \dots \cup C_m \quad (2)$$

A state vector \mathbf{x} satisfying $\nabla f(\mathbf{x}) = 0$ is called an *equilibrium vector* of f . An equilibrium vector \mathbf{x} is *hyperbolic* if the Hessian of f at \mathbf{x} restricted to the tangent space to \mathcal{X} at \mathbf{x} , denoted by $H_f(\mathbf{x})$, has no zero eigenvalues. A hyperbolic equilibrium vector \mathbf{x} is called an *index- k equilibrium vector* if $H_f(\mathbf{x})$ has k negative eigenvalues. The index corresponds to the dimension of the subspace consisting of directions in which f decreases. We denote an index- k equilibrium vector by \mathbf{x}^k .

A function f is a *Morse function* if all its equilibrium vectors are hyperbolic. Additionally, f is *separating* if distinct equilibrium vectors have distinct functional values. A basic result of Morse theory [17, 18] is that the class of the Morse functions forms an open, dense subset of all the smooth functions in the C^2 -topology, in other words, almost all smooth functions are

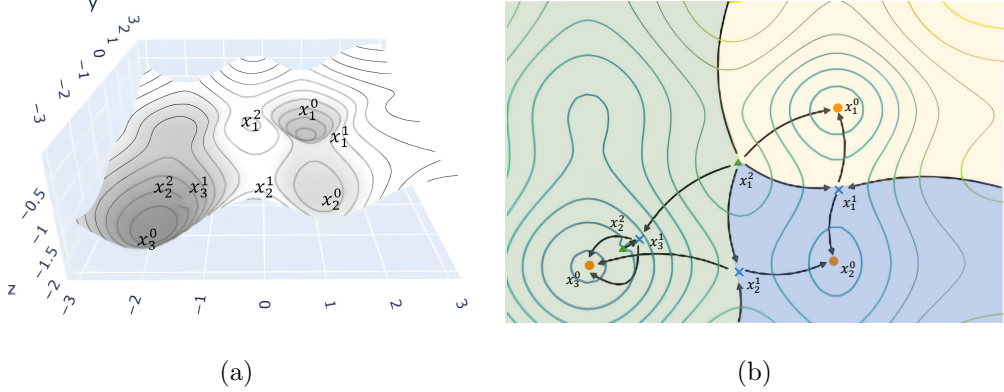


Figure 1: Illustration of Morse theory. (a) A three-dimensional surface plot of a toy example. (b) A level curve of (a). In (b), ‘o’s are stable equilibrium points, and ‘x’ refers to the index-1 equilibrium point. The triangle marker refers to the index-two equilibrium point. Note that x_3^1 is an index-1 equilibrium vector, but not a TEV.

Morse functions. Therefore, in this paper, it is assumed that the function considered is Morse, which is “generic”.

Morse theory addresses when the topology of $\#|\mathcal{X}_a|$ changes as a varies as follows: ($\#|A|$ denotes the number of connected components of a set A . See [17, 18] for more details.)

- $\#|\mathcal{X}_a|$ increases by one, i.e. $\#|\mathcal{X}_{a+\varepsilon}| = \#|\mathcal{X}_{a-\varepsilon}| + 1$ for a sufficiently small $\varepsilon > 0$, if and only if, $a \in \{f(\mathbf{x}_1^0), \dots, f(\mathbf{x}_s^0)\}$.
- $\#|\mathcal{X}_a|$ decreases by one, i.e. $\#|\mathcal{X}_{a+\varepsilon}| = \#|\mathcal{X}_{a-\varepsilon}| - 1$ for a sufficiently small $\varepsilon > 0$, if and only if, $a \in \{f(\mathbf{x}_1^1), \dots, f(\mathbf{x}_t^1)\}$ and also the following Morse relation holds.

$$\begin{aligned} H_0(\mathcal{X}_{a-\varepsilon}) &\cong H_0(\mathcal{X}_{a+\varepsilon}) \oplus \mathbb{R}, \\ H_q(\mathcal{X}_{a-\varepsilon}) &\cong H_q(\mathcal{X}_{a+\varepsilon}), \quad \text{for } q > 0 \end{aligned} \tag{3}$$

where $H_q(\cdot)$ is the q -th homology space and \cong implies homotopy equivalent. Such \mathbf{x}_i^1 are called *transition equilibrium vectors* (TEVs) (e.g., in Figure 1, \mathbf{x}_1^1 , \mathbf{x}_2^1 are TEVs, but \mathbf{x}_3^1 is not, as $\#\mathcal{X}$ remains constant despite being an index-1 equilibrium point).

- $\#\mathcal{X}_a$ remains constant, i.e., $\#\mathcal{X}_{a+\varepsilon} = \#\mathcal{X}_{a-\varepsilon}$ for a sufficiently small $\varepsilon > 0$, if and only if, a passes the value $f(\mathbf{x}^k)$ of an index- k equilibrium vector \mathbf{x}^k with $k > 1$.

4.2. Dynamical system perspective

Morse theory is not directly applicable due to the difficulty of computing the q -th homology space $H_q(\cdot)$, for example. The generalized gradient vector fields can help compute it [19]. Associated with the Morse function f , we can build the following generalized gradient system:

$$\frac{d\mathbf{x}}{dt} = -\text{grad}_R f(\mathbf{x}) \equiv -R(\mathbf{x})^{-1} \nabla f(\mathbf{x}). \quad (4)$$

where $R(\cdot)$ is a *Riemannian metric* on \mathcal{X} (i.e. $R(\mathbf{x})$ is a positive definite symmetric matrix for all $\mathbf{x} \in \mathcal{X}$). The existence of a unique solution (or trajectory) $\mathbf{x}(\cdot) : \mathbb{R} \rightarrow \mathcal{X}$ for each initial condition $\mathbf{x}(0)$ is guaranteed by the smoothness of f [20, 21] (i.e. f is twice differentiable). Without loss of generality, we assume that the trajectory $\mathbf{x}(\cdot)$ is defined for all $t \in \mathbb{R}$ for any initial condition $\mathbf{x}(0)$, achievable under a suitable re-parametrization [20].

A hyperbolic equilibrium vector is called an (asymptotically) *stable* equilibrium vector, denoted by \mathbf{x}^0 , if all eigenvalues of its corresponding Jacobian are positive, and an *unstable* equilibrium vector (or a *repellor*), denoted by \mathbf{x}^D , if all eigenvalues of its corresponding Jacobian are negative. A basic

result is that every local minimum of the Morse function f corresponds to an (asymptotically) stable equilibrium vector (SEV) of the system (4).

The (practical) *basin cell* of attraction of a SEV \mathbf{x}^0 is the closure of an open and connected stable manifold, defined by

$$\mathfrak{B}(\mathbf{x}^0) := \text{cl}(\{\mathbf{x}(0) \in \mathcal{X} : \lim_{t \rightarrow \infty} \mathbf{x}(t) = \mathbf{x}^0\}). \quad (5)$$

A basin cell groups similar data points through the system (4). Two SEVs, \mathbf{x}_i^0 and \mathbf{x}_j^0 , are *adjacent* if there exists an index-1 equilibrium vector $\mathbf{x}_{ij}^1 \in \mathfrak{B}(\mathbf{x}_i^0) \cap \mathfrak{B}(\mathbf{x}_j^0)$. It can be shown [22] that such an index-1 equilibrium vector is in fact a TEV between \mathbf{x}_a^0 and \mathbf{x}_b^0 that satisfies the Morse relation (3) and can be computed by using the system (4).

5. Proposed Method

Algorithm 1 Proposed Method

- 1: **Input:** Input data $\{\mathbf{x}_n\}_{n=1}^N \in [-1, 1]^{N \times D}$, privacy budget (ϵ, δ) , number of initial clusters K_0 , number of final clusters K , number of iterations τ_1, τ_2 , line search parameter m
- 2: **Output:** Final clusters $\{C\}_{k=1}^K$
- 3: $\{\pi_k, \boldsymbol{\mu}_k, \boldsymbol{\Sigma}_k\}_{k=1}^{K_0} \leftarrow \text{DPClustering}(\text{Input data}, \epsilon, \delta, K_0, \tau_1)$
- 4: Compute f from $\{\pi_k, \boldsymbol{\mu}_k, \boldsymbol{\Sigma}_k\}_{k=1}^{K_0}$
- 5: $G = (V, E) \leftarrow \text{TEVGraph}(\{\boldsymbol{\mu}_k\}_{k=1}^{K_0}, f, m, \tau_2)$
- 6: $\{C\}_{k=1}^K \leftarrow \text{MergeCluster}(G, K)$

The proposed method consists of three steps as summarized in Algorithm

1. First, differentially private parameters of the density function p , assumed

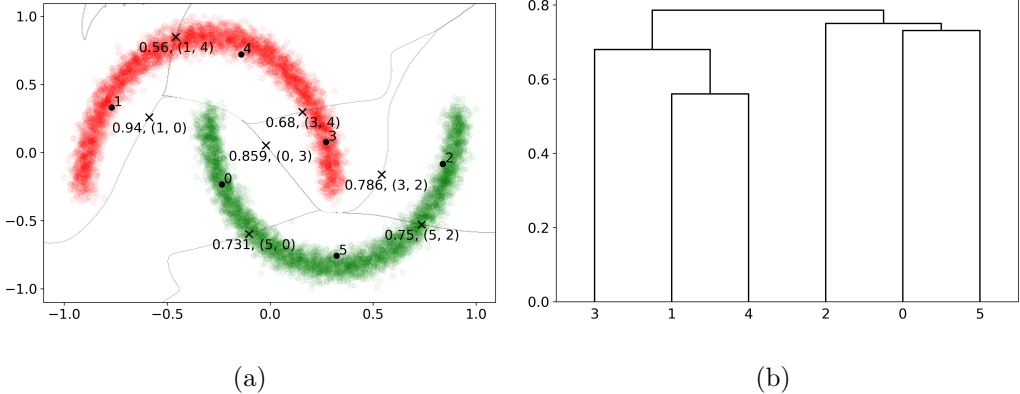


Figure 2: Description of the proposed dynamical processing. After obtaining an MoG density from textbf{DPCLustering}, (a) TEVs ('x') between adjacent centers (two numbers in parentheses) are identified, and the weight between two centers is calculated as the density (number at the bottom left) of the corresponding TEV. (b) A dendrogram is drawn based on the weighted graph. The x-axis denotes the index of centers, and the y-axis denotes the weight between the centers.

to be an MoG with K_0 clusters, are estimated from any existing method (line 3). We consider $-\ln p$ as the Morse function f . The centers of the MoG and their corresponding clusters effectively approximate SEVs and the associated basin cells, respectively. Subsequently, TEVs of f are identified according to (4), and a graph G is constructed (line 5). Finally, adjacent centers are connected until the desired number of clusters K is achieved (line 6). Figure 2 provides a visualization of the second and third steps.

5.1. Differentially private clustering

An MoG function can be represented as:

$$p(\mathbf{x}) = \sum_{k=1}^K \pi_k (2\pi)^{-\frac{D}{2}} |\Sigma_k|^{-\frac{1}{2}} e^{-\frac{1}{2}(\mathbf{x}-\mu_k)^T \Sigma_k^{-1} (\mathbf{x}-\mu_k)}, \quad (6)$$

where $\boldsymbol{\mu}_k \in \mathbb{R}^D$, $\boldsymbol{\Sigma}_k \in \mathbb{R}^{D \times D}$ are the mean and covariance of each normal distribution, and π_k is the probability of belonging to the k -th cluster. The associated MoG gradient system can be written as follows:

$$\frac{d\mathbf{x}}{dt} = R(\mathbf{x})^{-1} \nabla \ln p(\mathbf{x}) = -R(\mathbf{x})^{-1} \sum_{k=1}^K \omega_k(\mathbf{x}) \boldsymbol{\Sigma}_k^{-1}(\mathbf{x} - \boldsymbol{\mu}_k), \quad (7)$$

where $R(\cdot)$ is a *Riemannian metric* on \mathcal{X} and

$$\omega_k(\mathbf{x}) = \frac{\pi_k (2\pi)^{-\frac{D}{2}} |\boldsymbol{\Sigma}_k|^{-\frac{1}{2}} e^{-\frac{1}{2}(\mathbf{x} - \boldsymbol{\mu}_k)^T \boldsymbol{\Sigma}_k^{-1} (\mathbf{x} - \boldsymbol{\mu}_k)}}{\sum_{k=1}^K \pi_k (2\pi)^{-\frac{D}{2}} |\boldsymbol{\Sigma}_k|^{-\frac{1}{2}} e^{-\frac{1}{2}(\mathbf{x} - \boldsymbol{\mu}_k)^T \boldsymbol{\Sigma}_k^{-1} (\mathbf{x} - \boldsymbol{\mu}_k)}} > 0. \quad (8)$$

We focus on MoG density because the most studies are on k-means clustering or MoGs, from which the MoG density can be estimated.

5.1.1. Differentially private mixture of Gaussians

[5] proposed a differentially private MoG (DPMoG) method by adding noise to parameters μ_k, Σ_k, π_k in the M-step of the EM algorithm. Unlike k-means, MoG parameters are calculated using all samples, requiring larger noise proportional to the number of clusters, which degrades DPMoG's performance. Therefore, we present DPMoG-hard, a modified version whose performance is less affected by the number of clusters. To enable parallel composition, we transform the responsibility obtained in the E step so each sample is assigned with a probability of 1 to a single cluster. This technique, known as hard EM [23], is first applied to enhance DP. DPMoG-hard is an instantiation of **DPClustering** in Algorithm 1.

The detailed procedure of DPMoG-hard is presented in Algorithm 2. For the mathematical formulation of this algorithm, refer to [5]. Specifying a distribution (lines 9, 12-14) implies performing random sampling from that

Algorithm 2 DPMoG-hard: An instantiation of DPCLustering

- 1: **Input:** Input data $\{\mathbf{x}_n\}_{n=1}^N \in [-1, 1]^{N \times D}$, privacy budget (ϵ, δ) , number of clusters K , number of iterations τ
- 2: **Output:** Parameters $\{\pi_k^\tau\}_{k=1}^K, \{\boldsymbol{\mu}_k^\tau\}_{k=1}^K, \{\boldsymbol{\Sigma}_k^\tau\}_{k=1}^K$
- 3: Initialize parameters $\{\pi_k^0\}_{k=1}^K, \{\boldsymbol{\mu}_k^0\}_{k=1}^K, \{\boldsymbol{\Sigma}_k^0\}_{k=1}^K$
- 4: $r \leftarrow 1 + 3D + 2D^2; \quad \sigma \leftarrow \sqrt{\frac{r\tau}{2}} \frac{\sqrt{\log(1/\delta) + \epsilon} + \sqrt{\log(1/\delta)}}{\epsilon}$ // Calculate from 9
- 5: $C_k \leftarrow \emptyset, \quad k = 1, \dots, K$
- 6: **for** $t = 1$ to τ **do**
- 7: **for** $n = 1$ to N **do**
- 8: **for** $k = 1$ to K **do**
- 9: $\gamma_{nk}^t \leftarrow \pi_k^{t-1} \mathcal{N}(\mathbf{x}_n | \boldsymbol{\mu}_k^{t-1}, \boldsymbol{\Sigma}_k^{t-1}) / \sum_{l=1}^K \pi_l^{t-1} \mathcal{N}(\mathbf{x}_n | \boldsymbol{\mu}_l^{t-1}, \boldsymbol{\Sigma}_l^{t-1})$
- 10: $k^* = \arg \max_k \gamma_{nk}^t; \quad C_{k^*} \leftarrow C_{k^*} \cup \{n\}$ // hard EM
- 11: **for** $k = 1$ to K **do**
- 12: $N_k \leftarrow |C_k| + \mathcal{N}(0, \sigma^2); \quad \pi_k^t \leftarrow N_k / N$
- 13: $\boldsymbol{\mu}_k^t \leftarrow \frac{1}{N_k} (\sum_{n \in C_k} \mathbf{x}_n + \mathcal{N}(\mathbf{0}, \sigma^2 \mathbf{I}_D))$
- 14: $\boldsymbol{\Sigma}_k^t \leftarrow \frac{1}{N_k} (\sum_{n \in C_k} (\mathbf{x}_n - \boldsymbol{\mu}_k^t)(\mathbf{x}_n - \boldsymbol{\mu}_k^t)^T + \text{sym}(\mathcal{N}(\mathbf{0}, \sigma^2 \mathbf{I}_{D(D+1)/2})))$

distribution. sym transforms a $D(D+1)/2$ -dimensional vector into a $D \times D$ -dimensional symmetric matrix.

Using the composition theorem, Algorithm 2 satisfies (ϵ, δ) -DP by setting σ as specified in line 3. Due to DPMoG-hard's hard clustering nature, the parallel composition theorem ensures that the total privacy loss remains unaffected by the number of clusters, K .

Proposition 5.1. *Algorithm 2 is (ϵ, δ) -differentially private.*

Proof. The sensitivity of $|C_k|$ is 1, and the sensitivity of each coordinate of

$\sum_{n \in C_k} \mathbf{x}_n$ is 2. $\sum_{n \in C_k} \mathbf{x}_n \mathbf{x}_n^T$ has $D(D + 1)/2$ unique elements. While D diagonal elements have sensitivity 1, the others have sensitivity 2.

Using remark 3.4 and 3.5, it can be directly shown that for an iteration,

- N_k is $(1/2\sigma^2)$ -zCDP,
- $\sum_{n \in C_k} \mathbf{x}_n + \mathcal{N}(\mathbf{0}, \sigma^2 \mathbf{I}_D)$ is $(2^2 D/2\sigma^2)$ -zCDP,
- $\sum_{n \in C_k} (\mathbf{x}_n - \boldsymbol{\mu}_k^t)(\mathbf{x}_n - \boldsymbol{\mu}_k^t)^T + \text{sym}(\mathcal{N}(\mathbf{0}, \sigma^2 \mathbf{I}_{D(D+1)/2}))$ is $(D/2\sigma^2)$ -zCDP for diagonal elements and $(2^2 D(D - 1)/4\sigma^2)$ -zCDP for the others.

By remark 3.5, τ iterations of the algorithm is $(1 + 3D + 2D^2)\tau/2\sigma^2$ -zCDP.

According to remark 3.2, Algorithm 2 is (ϵ, δ) -DP with

$$\sigma = \sqrt{\frac{r\tau}{2} \frac{\sqrt{\log(1/\delta)} + \epsilon + \sqrt{\log(1/\delta)}}{\epsilon}}, \quad (9)$$

where $r = 1 + 3D + 2D^2$. \square

5.1.2. Differentially private k-means clustering

There have been various studies on k-means clustering algorithms that satisfy DP [24, 3, 4]. Despite differences in privacy and utility analysis, our approach can be applied to any of them since they all output centers and allocate samples to centers. However, k-means clustering does not directly provide a density function. To address this, we build a Gaussian density function by calculating the covariance matrix of each cluster and using it as Σ_k of each Gaussian distribution. As in the last line of Algorithm 2, noise is when calculating the covariance matrices to ensure DP, causing a little additional privacy loss.

5.2. Transition equilibrium vectors and the weighted graph

To generate clusters of arbitrary shapes using the system (7), we group similar basin cells based on mutual proximity or dissimilarity. Using adjacent SEVs and TEVs, we construct the weighted graph $G = (V, E)$ with a derived distance [10]:

1. The vertices V of G are the SEVs, $\mathbf{x}_1^0, \dots, \mathbf{x}_s^0$, $i = 1, \dots, s$ of (4).
2. The edge E of G connect vertices of adjacent SEVs, $\mathbf{x}_i^0, \mathbf{x}_j^0$, with weights $d_E(\mathbf{x}_i^0, \mathbf{x}_j^0) := f(\mathbf{x}_{ij}^1)$, where \mathbf{x}_{ij}^1 is a TEV between them.

For \mathcal{X}_a , we then construct a sub-graph $G_a = (V_a, E_a)$ with:

1. The vertices $V_a \subset V$ of G_a consists of SEVs, \mathbf{x}_i^0 , in V with $f(\mathbf{x}_i^0) < a$.
2. The edge $E_a \subset E$ of G_a consists of $(\mathbf{x}_i^0, \mathbf{x}_j^0) \in E$ with $d_E(\mathbf{x}_i^0, \mathbf{x}_j^0) < a$.

Since the distance metric is based on the density function, it describes the data distribution more effectively than Euclidean distance methods. It also efficiently partitions the entire data space [10]. We generalize the results from [10] using the Riemannian metric in the context of MoG (Theorem 5.3).

The next result shows the equivalence between the topological structures of G_a and the connected components of \mathcal{X}_a .

Proposition 5.2. [25] *With respect to the MoG (6), \mathbf{x}_i^0 and \mathbf{x}_j^0 are in the same connected component of the sub-graph G_a if, and only if, \mathbf{x}_i^0 and \mathbf{x}_j^0 are in the same cluster of the level set \mathcal{X}_a , that is, each connected component of G_a corresponds to a cluster of \mathcal{X}_a .*

Morse theory ensures a TEV exists between two adjacent SEVs for any Morse function. Since the distance d_E is defined by the function value of the TEV, connecting SEVs based on this distance constructs a new sub-graph with a modified value of a . Thus, we can efficiently construct an optimal sub-graph for clustering data based on the partitioned data manifold.

The next result shows an inductive property of the system (7), which allows to assign a label to a new test point without retraining. This naturally partitions the sample space by assigning points in different basin cells to their respective SEVs. Conversely, traditional density-based clustering methods require retraining to label a new test point, wasting the privacy budget.

Theorem 5.3 (Inductive Property). *Suppose that the Riemannian metric $R(\cdot)$ on \mathcal{X} of the associated MoG gradient system (7) has a finite condition number. Then the whole data space is almost surely a pairwise disjoint union of the basin cells $\mathfrak{B}(\mathbf{x}_i^0)$ where $\mathbf{x}_i^0|_{i \in \{1, \dots, s\}}$ are the SEVs of the system (7), i.e.*

$$\mathcal{X} = \mathfrak{B}(\mathbf{x}_1^0) \dot{\cup} \dots \dot{\cup} \mathfrak{B}(\mathbf{x}_s^0). \quad (10)$$

Here, an almost surely disjoint union $A \dot{\cup} B$ of two nonempty sets A and B means that $A \cap B$ has a Lebesgue measure zero.

Proof. Following the proof of Lasalle's invariance property theorem [20, 21], it can be easily shown that every bounded trajectory of the system (7) converges to one of the equilibrium vectors. Therefore it is enough to show that every trajectory is bounded.

Since $R(\mathbf{x})^{-1}$ and Σ_k^{-1} are positive definite, we can let $A_k(\mathbf{x})$ be the Cholesky factorization of the positive definite matrix $R(\mathbf{x})^{-1}\Sigma_k^{-1}$ that satisfies $R(\mathbf{x})^{-1}\Sigma_k^{-1} = A_k(\mathbf{x})^T A_k(\mathbf{x})$. Then $(\mathbf{x}^T R(\mathbf{x})^{-1}\Sigma_k^{-1}\mathbf{x}) = \|A_k(\mathbf{x})\mathbf{x}\|^2$. Since

the condition number of $R(\mathbf{x})$ is bounded, by the spectral theorem, there exist smooth eigenvalue functions $\lambda_{\min}^k(\mathbf{x}), \lambda_{\max}^k(\mathbf{x}) > 0$ and $\gamma > 0$ such that

$$\|A_k(\mathbf{x})\| = \sqrt{\lambda_{\max}^k(\mathbf{x})}, \quad \forall k = 1, \dots, K, \quad \forall \mathbf{x} \in \mathcal{X}, \quad (11)$$

$$\kappa(A_k(\mathbf{x})) := (\lambda_{\max}^k(\mathbf{x})/\lambda_{\min}^k(\mathbf{x}))^{1/2} \leq \gamma, \quad \forall k = 1, \dots, K, \quad \forall \mathbf{x} \in \mathcal{X} \quad (12)$$

where $\|\cdot\|$ denotes the Euclidean- or ℓ_2 -norm. Now let $V(\mathbf{x}) = \frac{1}{2}\|\mathbf{x}\|^2$ and choose $\Upsilon > \gamma \max_k \|\boldsymbol{\mu}_k\|$. Then for any $L > \Upsilon$, and for all $\|\mathbf{x}\| = L$, we have

$$\begin{aligned} \frac{\partial}{\partial t} V(\mathbf{x}) &= \mathbf{x}^T \frac{d\mathbf{x}}{dt} = -\mathbf{x}^T \sum_k \omega_k(\mathbf{x}) R(\mathbf{x})^{-1} \Sigma_k^{-1} (\mathbf{x} - \boldsymbol{\mu}_k) \\ &= -\mathbf{x}^T \sum_k \omega_k(\mathbf{x}) R(\mathbf{x})^{-1} \Sigma_k^{-1} \mathbf{x} + \mathbf{x}^T \sum_k \omega_k(\mathbf{x}) R(\mathbf{x})^{-1} \Sigma_k^{-1} \boldsymbol{\mu}_k \\ &= -\sum_k \omega_k(\mathbf{x}) \mathbf{x}^T A_k(\mathbf{x})^T A_k(\mathbf{x}) \mathbf{x} + \sum_k \omega_k(\mathbf{x}) \mathbf{x}^T A_k(\mathbf{x})^T A_k(\mathbf{x}) \boldsymbol{\mu}_k \\ &\leq -\sum_k \omega_k(\mathbf{x}) \|A_k(\mathbf{x}) \mathbf{x}\|^2 + \sum_k \omega_k(\mathbf{x}) \|A_k(\mathbf{x}) \mathbf{x}\| \|A_k(\mathbf{x}) \boldsymbol{\mu}_k\| \\ &= \sum_k \omega_k(\mathbf{x}) \|A_k(\mathbf{x}) \mathbf{x}\| (\|A_k(\mathbf{x}) \boldsymbol{\mu}_k\| - \|A_k(\mathbf{x}) \mathbf{x}\|) \\ &\leq \sum_k \omega_k(\mathbf{x}) \|A_k(\mathbf{x}) \mathbf{x}\| (\sqrt{\lambda_{\max}^k(\mathbf{x})} \|\boldsymbol{\mu}_k\| - \sqrt{\lambda_{\min}^k(\mathbf{x})} \|\mathbf{x}\|) < 0 \end{aligned}$$

Therefore, for any $L > \Upsilon$, the trajectory starting from any point on $\|\mathbf{x}\| = L > \Upsilon$ always enters into the bounded set $\|\mathbf{x}\| \leq L$, which implies that $\{\mathbf{x}(t) : t \geq 0\}$ is bounded. \square

Algorithm 3 demonstrates the procedures for finding TEVs and the weighted graph G . The input f is a density function obtained from **DPClustering**. For example, p can be computed using (6) from $\{\pi_k\}, \{\boldsymbol{\mu}_k\}, \{\boldsymbol{\Sigma}_k\}$ output by Algorithm 2, with $f = -\ln p$. m and τ , are hyperparameters. We use the centers $\{\boldsymbol{\mu}_k\}$ instead of SEVs, as the density of a center is very close to the local minimum, indicating an SEV nearby. This approach omits additional steps to find SEVs, saving computation time compared to previous studies.

To find TEVs, we present an efficient modification of the quadratic string search method in [26]. We constrain \mathbf{m}^{t-1} from the last iteration to be the vertex of the quadratic function $y = -x^2 + x$ in the transformed coordinates, where the two centers form the unit vector from on the x-axis. We split \mathbf{u} into $m + 1$ intervals and calculate the corresponding points on the quadratic function for each vertex of the interval. Then, we find the point with the smallest density and iterate (7) from this point to compute \mathbf{m}^t (line 9-12). Figure 3 illustrates this procedure. The remaining parts of the algorithm identifies the index-1 equilibrium vectors from the TEV candidates (line 16) and filters TEVs satisfying (3) (lines 17-20). The next result shows the dynamical invariance property of the MoG system (7) that preserves DP, implying that Algorithm 3 does not incur any additional privacy loss.

Theorem 5.4 (Preserving Differential Privacy). *Let \mathcal{M} with $\text{Range}(\mathcal{M}) \subseteq \mathcal{X}$ be a randomized algorithm that is (ϵ, δ) -differentially private. Then under the same condition of Theorem 5.3, the inductive dynamical processing (7) applied to \mathcal{M} is (ϵ, δ) -differentially private, i.e. the solution trajectory $\mathbf{x}(t)$ of the MoG gradient system (7) with initial condition $\mathbf{x} \in \mathcal{M}$ is (ϵ, δ) -differentially private.*

Proof. Define the flow $\Phi_t : \mathcal{X} \rightarrow \mathcal{X}$ of the MoG gradient system (7) by $\Phi_t(\mathbf{x}) = \mathbf{x}(t)$ with initial condition $\mathbf{x}(0) = \mathbf{x}$ for $t \in \mathbb{R}$. Then by the fundamental theorem of the flow defined by the system (7), we have $\Phi_{s+t}(\mathbf{x}) = \Phi_s \circ \Phi_t(\mathbf{x})$ for all $\mathbf{x} \in \mathcal{X}$ and $s, t \in \mathbb{R}$. (See [21] for more details.) Now let a pair of neighboring databases D_1, D_2 with $\|D_1 - D_2\|_1 \leq 1$ be given. Then

Algorithm 3 TEVGraph

1: **Input:** Centers $\{\boldsymbol{\mu}_k\}_{k=1}^K$, density function f , line search parameter m , number of iterations τ

2: **Output:** Weighted graph $G = (V, E)$

3: $V \leftarrow \{\boldsymbol{\mu}_k\}_{k=1}^K$; $T \leftarrow \emptyset$

4: **for** $k = 1$ to K **do**

5: **for** $l = k + 1$ to K **do**

6: $i^* \leftarrow \arg \max_{i \in \{1, \dots, m\}} f(\mu_k + \frac{i}{m+1}(\mu_l - \mu_k))$

7: $\mathbf{m}^0 \leftarrow \mu_k + \frac{i^*}{m+1}(\mu_l - \mu_k)$; $\mathbf{m}^0 \leftarrow \text{Integrate (7) from } \mathbf{m}^0$

8: **for** $t = 1$ to τ **do**

9: $\mathbf{u} \leftarrow \boldsymbol{\mu}_l - \boldsymbol{\mu}_k$; $\mathbf{v} \leftarrow \mathbf{m}^0 - \boldsymbol{\mu}_k$

10: $i^* \leftarrow \arg \max_{i \in \{1, \dots, m\}} f(\mu_k + \frac{i}{m+1}\mathbf{u} + (\frac{i}{m+1} - (\frac{i}{m+1})^2)(4\mathbf{v} - 2\mathbf{u}))$

11: $\mathbf{m}^t \leftarrow \mu_k + \frac{i^*}{m+1}\mathbf{u} + (\frac{i^*}{m+1} - (\frac{i^*}{m+1})^2)(4\mathbf{v} - 2\mathbf{u})$

12: $\mathbf{m}^t \leftarrow \text{Integrate (7) from } \mathbf{m}^t$

13: $\mathbf{t}_{tmp} \leftarrow \text{Find the solution of } \nabla f(\mathbf{x}) = 0 \text{ from } \mathbf{m}^t$

14: $T \leftarrow T \cup \{\mathbf{t}_{tmp}\}$

15: **for** $\mathbf{t} \in T$ **do**

16: **if** Hessian $\nabla^2 f(\mathbf{t})$ has one negative eigenvalue **then**

17: $\mathbf{e} \leftarrow \text{Eigenvector corresponding to the negative eigenvalue}$

18: $\mathbf{x}_0 \leftarrow \mathbf{t} + \varepsilon \mathbf{e}$; $\mathbf{x}_1 \leftarrow \mathbf{t} - \varepsilon \mathbf{e}$ for small $\varepsilon > 0$

19: $\boldsymbol{\mu}_0, \boldsymbol{\mu}_1 \leftarrow \text{Numerically integrate (7) from } \mathbf{x}_0, \mathbf{x}_1$

20: **if** $\boldsymbol{\mu}_0 \neq \boldsymbol{\mu}_1$ **then**

21: $E \leftarrow E \cup \langle \boldsymbol{\mu}_0, \boldsymbol{\mu}_1, f(\mathbf{t}) \rangle$

for all $\mathbf{x} \in \mathcal{M}(D_1)$

$$\mathbf{x}(t) = \Phi_t \circ \Phi_0(\mathbf{x}) = \Phi_t \circ \mathbf{x}(0) \quad (13)$$

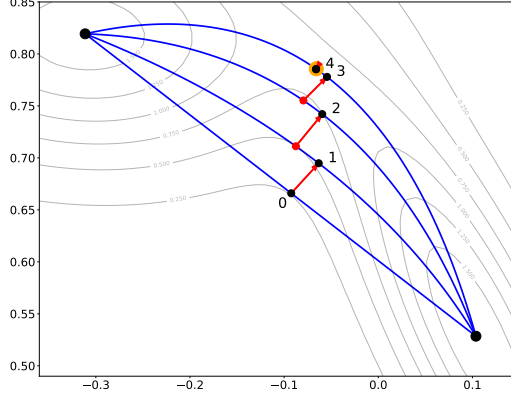


Figure 3: Procedure to find TEVs. Big black points are MoG centers, and the big orange point is the TEV. Small black points with numbers represent \mathbf{m}^t at step t , and small red points indicate minimum density points on the quadratic string.

For any event $\mathcal{O} \subset \text{Range}(\mathcal{M}) \subseteq \mathcal{X}$ and any $t \in \mathbb{R}$, we let $\mathcal{W}_t = \{\mathbf{x} \in \mathcal{X} : \mathbf{x}(t) \in \mathcal{O}\}$. Then we have

$$\begin{aligned}
 \Pr\{\mathbf{x}(t) \in \mathcal{O} : \mathbf{x} \in \mathcal{M}(D_1)\} &= \Pr[\mathcal{M}(D_1) \in \mathcal{W}_t] \\
 &\leq e^\epsilon \Pr[\mathcal{M}(D_2) \in \mathcal{W}_t] + \delta \\
 &= e^\epsilon \Pr\{\mathbf{x}(t) \in \mathcal{O} : \mathbf{x} \in \mathcal{M}(D_2)\} + \delta
 \end{aligned} \tag{14}$$

Since this result works for any $t \in \mathbb{R}$, the inductive dynamical processing applied to \mathcal{M} by system (7) is (ϵ, δ) -differentially private. \square

5.3. Hierarchical merging of sub-clusters

In the final step, sub-clusters are hierarchically merged until the desired number of clusters is achieved, using the weighted graph obtained in the previous step. Let the number of clusters, K , be arbitrarily given. The method begins with each center representing a singleton cluster. The detailed procedure is demonstrated in Algorithm 4. Denote these clusters

$C_1 = \{\boldsymbol{\mu}_1\}, \dots, C_L = \{\boldsymbol{\mu}_L\}$. At each step, the two separate clusters containing two adjacent SEVs with the smallest edge weight distance are merged into a single cluster (lines 10-11), producing one less cluster at the next higher level (lines 12-13). This process continues until K clusters are obtained from the initial L clusters (line 9). Since Algorithm 4 operates only on the centers and TEVs, which preserve DP, it inherently maintains (ϵ, δ) -DP by the post-processing property.

Another feature of the MoG system is its agglomerative property, i.e. system (7) can construct a hierarchy of clusters starting from the basin cells. This ensures that Algorithm 4 can achieve any number of clusters.

Theorem 5.5 (Agglomerative Property). *Let $\mathbf{x}_i^0, i = 1, \dots, s$ and $\mathbf{x}_j^1, j = 1, \dots, t$ be the SEVs and the TEVs of the MoG system (7), respectively. Consider an agglomerative process such that each basin cell $\mathfrak{B}(\mathbf{x}_1^0)$ starts in its own cluster and a pair of clusters are merged when the two separate clusters contain adjacent basin cells with the least edge weight $f(\mathbf{x}_j^1)$. Then the merging occurs when we decrease the level value a starting from $\max_i f(\mathbf{x}_i^0)$ until it hits the value in $\{f(\mathbf{x}_1^1), \dots, f(\mathbf{x}_t^1)\}$ and this process is terminated when we get one cluster, say \mathcal{X} , starting from s clusters.*

Proof. The first part of the proof comes from the Morse theory. For the second part of the proof, it is sufficient to show that $\eta > 0$ exists, with \mathcal{X}_r connected for all $0 < r < \eta$. From the Cholesky factorization of Σ_k^{-1} , we can let $\Sigma_k^{-1} = U_k^T U_k$ where U_k is an upper triangle matrix with positive diagonal elements. By the singular value decomposition theorem, $0 < \sigma_d^{(k)} \|\mathbf{x}\| \leq \|U_k \mathbf{x}\| \leq \sigma_1^{(k)} \|\mathbf{x}\|$ where $\sigma_1^{(k)} \geq \dots \geq \sigma_d^{(k)}$ are the singular val-

Algorithm 4 MergeCluster

- 1: **Input:** Weighted graph $G = (V, E)$, number of clusters K
- 2: **Output:** Clusters $\{C\}_{k=1}^K$
- 3: $L \leftarrow |V|$, $C_1 \leftarrow \{\boldsymbol{\mu}_1\}, \dots, C_L \leftarrow \{\boldsymbol{\mu}_L\}$
- 4: **if** $\langle \boldsymbol{\mu}_i, \boldsymbol{\mu}_j, f(\mathbf{t}) \rangle \in E$ **then**
- 5: $d(C_i, C_j) \leftarrow f(\mathbf{t})$
- 6: **else**
- 7: $d(C_i, C_j) \leftarrow \infty$
- 8: **for** $l = 1$ to $L - K$ **do**
- 9: Find the smallest d and the corresponding C_a, C_b
- 10: $C_{L+l} \leftarrow C_a \cup C_b$ // Merge two adjacent SEVs as in 5.3
- 11: $d(C_{L+1}, C_c) = \min\{d(C_a, C_c), d(C_b, C_c)\}$ for all remaining C_c s
- 12: Remove C_a and C_b

ues for $k = 1, \dots, K$. Let $a := \min_k \sigma_d^{(k)}$, $b := \max_k \sigma_1^{(k)}$. Choose $\zeta > \max\{\frac{b}{a}, \gamma\} \cdot \max_k \|\boldsymbol{\mu}_k\|$, then for all $\|\mathbf{x}\| = L > \zeta$, we have

$$\|U_k(\mathbf{x} - \boldsymbol{\mu}_k)\| \leq \|U_k \mathbf{x}\| + \|U_k \boldsymbol{\mu}_k\| < bL + \frac{a\sigma_1^{(k)}}{b}L \leq (b+a)L, \quad (15)$$

By the proof of Theorem 5.3, every trajectory starting from $\|\mathbf{x}\| = L$ for any $L > \zeta$ always enters into $\mathcal{S}_L := \{\mathbf{x} : \|\mathbf{x}\| \leq L\}$, a connected and bounded set. It is enough to show that there exists a $\eta > 0$ such that $\mathcal{S}_L \subset \mathcal{X}_\eta$.

$$\begin{aligned} p(\mathbf{x}) &= \sum_{k=1}^K \pi_k (2\pi)^{-\frac{d}{2}} |\boldsymbol{\Sigma}_k|^{-\frac{1}{2}} e^{-\frac{1}{2}(\mathbf{x} - \boldsymbol{\mu}_k)^T \boldsymbol{\Sigma}_k^{-1} (\mathbf{x} - \boldsymbol{\mu}_k)} \\ &> \sum_{k=1}^K \pi_k (2\pi)^{-\frac{d}{2}} |U_k| e^{-\frac{1}{2}(a+b)^2 L^2} \\ &\geq (2\pi/a^2)^{-\frac{d}{2}} e^{-\frac{1}{2}(a+b)^2 L^2}. \end{aligned} \quad (16)$$

The last inequality follows from $\sum_{k=1}^K \pi_k = 1$ and $|U_k| = \prod_{i=1}^d \sigma_i^{(k)} \geq (\sigma_d^{(k)})^d \geq a^d$. When we choose $\eta = (2\pi/a^2)^{-\frac{d}{2}} e^{-\frac{1}{2}(a+b)^2 L^2}$, we have $\mathcal{S}_L \subset \mathcal{X}_r$ for all $0 < r < \eta$. Hence, by theorem 5.3, for any point $\mathbf{x}_0 \in (\mathcal{X}_r \setminus \mathcal{S}_L)$, every trajectory starting from \mathbf{x}_0 should hit the boundary L and enters into the region \mathcal{S}_L . This implies that the set \mathcal{S}_L is a strong deformation retract of the level set \mathcal{X}_r , which shows that \mathcal{X}_r is connected for all $r < \gamma$. \square

This last step possesses a monotonicity property, meaning the dissimilarity between merged clusters increases monotonically with the level of the merger. As a result, a dendrogram can be plotted so that the height of each node is proportional to the inter-group dissimilarity value between its two daughters. The dendrogram is illustrated in Figure 2(b).

6. Experiments

We evaluate the proposed method on various real-world datasets to verify that our method achieves better clustering results than existing methods.

6.1. Datasets

Six datasets were employed in this study: **Shuttle**, EMG physical action (**EMG**), MAGIC gamma telescope (**MAGIC**) from the UCI Machine Learning Repository [27], Sloan digital sky survey (**Sloan**), Predicting pulsar star (**Pulsar**), and **USPS** from Kaggle¹ competitions. To ensure DP, all variables were rescaled to the range of $[-1, 1]$. The **EMG** dataset, originally with 10 classes, was modified by excluding similar actions. For the **USPS**

¹<https://www.kaggle.com>

Table 1: Description of datasets.

Dataset	# of samples (N)	# of variables (D)	# of clusters (K)	# of sub-clusters (K_0)
Shuttle	43500	9	7	12
EMG	59130	8	6	10
MAGIC	19020	10	2	6
Sloan	10000	16	3	6
Pulsar	9273	8	2	6
USPS	7291	3	10	13

dataset, dimensionality was reduced from 16×16 to 3 using t-SNE. A detailed overview of the datasets is in Table 1.

6.2. Details on experiments

We employed the following four baseline methodologies:

- **DPMoG-hard**: The proposed differentially private MoG method outlined in Algorithm 2.
- **DPLloyd** [28]²: A differentially private adaptation of the Lloyd algorithm for k-means clustering.
- **DPCube** [29]³: A recent differentially private clustering approach designed for high-dimensional data.
- **DPTree** [30]⁴: Generating a differentially private coresset algorithm.

²<https://github.com/DongSuIBM/PrivKmeans>

³<https://github.com/mouwenlong/dp-clustering-icml17>

⁴<https://github.com/google/differential-privacy/tree/main/learning/clustering>

To the best of our knowledge, we incorporated all methods with available source code. Other studies on differentially private k-means clustering primarily focus on theoretical utility without providing empirical validations or publicly available code. Note that each baseline method can be treated as an instantiation of **DPClustering** in Algorithm 1.

To demonstrate the applicability of the proposed method (Algorithm 1) across various baseline methods, we conducted a comparative analysis of these methods before and after the application of the proposed framework. For clarity, we denoted the application of the proposed method by appending ‘**-Morse**’ to each method’s name. For instance, using **DPMoG-hard** as **DPClustering**, the proposed method was referred to as **DPMoG-hard-Morse**. We then compared the clustering metrics of **DPMoG-hard** with **DPMoG-hard-Morse**, extending this comparison to all baseline methods.

For k-means clustering methods, additional privacy loss is incurred when privately calculating covariance matrices. The allocation of the privacy budget to covariance calculation is flexible. For example, in **DPLloyd-Morse**, ρ for zCDP is assigned proportionally to the number of elements requiring added noise. Due to the increased complexity of algorithms for **DPCube** and **DPTree** compared to **DPLloyd**, line searches were conducted for these methods to determine the optimal distribution of the privacy budget.

The clustering metric used in the evaluation was the adjusted Rand index (ARI), which ranges from 0 and 1, with values closer to 1 indicating superior clustering. While ARI typically requires true labels, alternative clustering metrics that do not depend on true labels, such as silhouette scores, were found unsuitable for capturing complex cluster shapes.

The total privacy budget ϵ was set to $\{10, 5, 2, 1, 0.5\}$. For $\epsilon < 0.5$, baseline methods exhibited low ARI scores for most datasets, contrasting with experiments using other metrics such as the k-means objective, where performance is retained for smaller ϵ . For **DPMoG-hard** and **DPMoG-hard-Morse**, $\epsilon = 0.5$ were excluded due to their suboptimal performance.

All the experiments were performed on a machine with 48 threads of Intel Xeon CPU E5-2680 v3 @ 2.50GHz CPU. The experiments were conducted using Python 3.6.9, repeated five times, and the average results were obtained. In addition to the privacy budget ϵ , several parameters were determined. The number of iterations τ_1 and τ_2 were set to 10 and 5, respectively, for all experiments. In Algorithm 3, m and ε were set to 20 and 0.05, respectively.

6.3. Effectiveness of dynamical processing

6.3.1. Results on differentially private mixture of Gaussians

The clustering outcomes of **DPMoG-hard** and **DPMoG-hard-Morse** for the six datasets are illustrated in Figure 4. The application of Morse theory in **DPMoG-hard-Morse** consistently yields higher ARI values compared to **DPMoG-hard**. Notably, in the case of **Pulsar** dataset, ARI exhibits a notable increase of up to 0.2, signifying a substantial enhancement. For the other datasets, ARI generally increases by 0.05 to 0.1. These results suggest that the proposed method effectively merges the generated sub-clusters to accurately represent clusters with arbitrary shapes.

However, for most datasets, the disparity in ARI scores between **DPMoG-hard** and **DPMoG-hard-Morse** tends to diminish as ϵ decreases. Additionally, for the **EMG** and **Sloan** datasets, the improvement is relatively modest across all values of ϵ . Both datasets consistently exhibit suboptimal

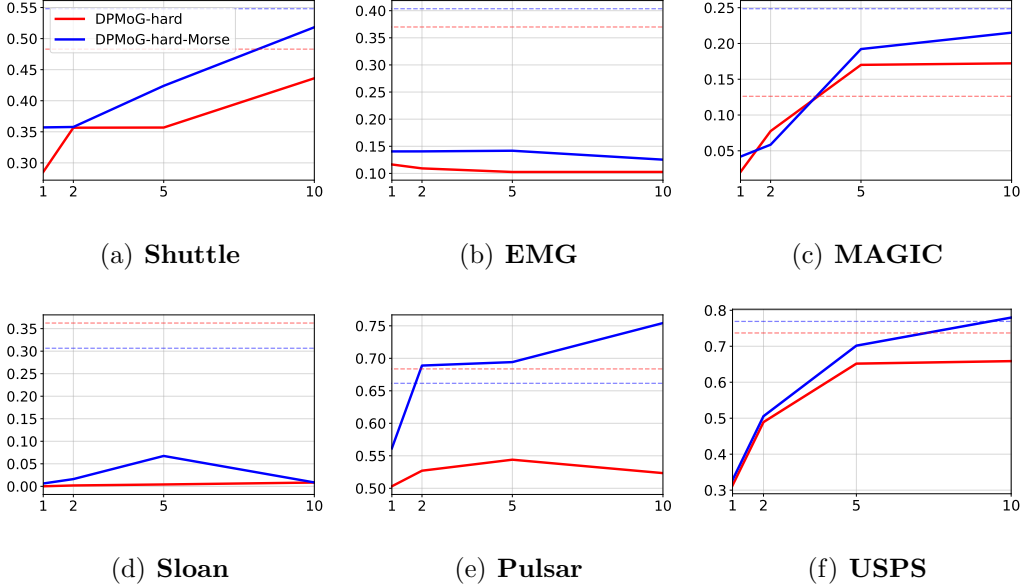


Figure 4: Clustering results of **DPMoG-hard** and **DPMoG-hard-Morse** for real-world datasets. The x-axis indicates the privacy budget ϵ , and the y-axis indicates the ARI score. The dotted lines indicate the performances of the non-private models.

performance compared to the non-private model even at $\epsilon = 10$. This suggests a limitation of the proposed method, wherein the application of Morse theory does not significantly enhance performance when the performance of the baseline model is already severely compromised by noise to ensure DP.

6.3.2. Results on differentially private k-means

Figure 5 compares the clustering outcomes between **DPLlloyd** and **DPLlloyd-Morse** across the same six datasets. In nearly all instances, the ARI score of **DPLlloyd-Morse** surpasses that of **DPLlloyd**. Furthermore, akin to the observations for **DPMoG-hard**, the distinction in ARI scores between **DPLlloyd** and **DPLlloyd-Morse** diminishes with decreasing ϵ . Specifically, for datasets such as **Shuttle**, **Magic**, **Pulsar**, and **USPS**, where ARI scores

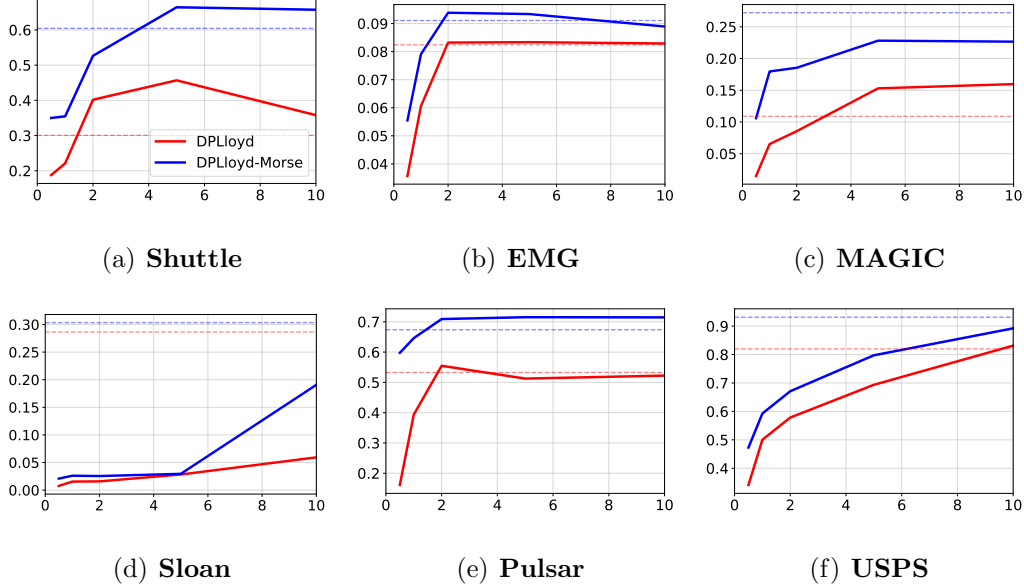


Figure 5: Clustering results of **DPLlloyd** and **DPLlloyd-Morse** for real-world datasets. The x-axis indicates the privacy budget ϵ , and the y-axis indicates the ARI score. The dotted lines indicate the performances of the non-private models.

of **DPLlloyd** exhibit moderate performance, the difference in ARI scores between **DPLlloyd-Morse** and **DPLlloyd** consistently proves to be significant, indicating a notable enhancement. Although the absolute improvement is marginal for **EMG** and **Sloan**, where **DPLlloyd** demonstrates suboptimal ARI scores, the ratio between the ARI scores is found to be sufficiently substantial (at least a 12% increase in most cases).

Figure 6 illustrates the outcomes of **DPCube** and **DPCube-Morse**. Notably, **DPCube-Morse** consistently exhibits superior clustering performance compared to **DPCube** in regions characterized by higher privacy levels (larger values of ϵ). In the case of **EMG** dataset, **DPCube** outperforms **DPCube-Morse** when $\epsilon \leq 2$, though the difference is not significant

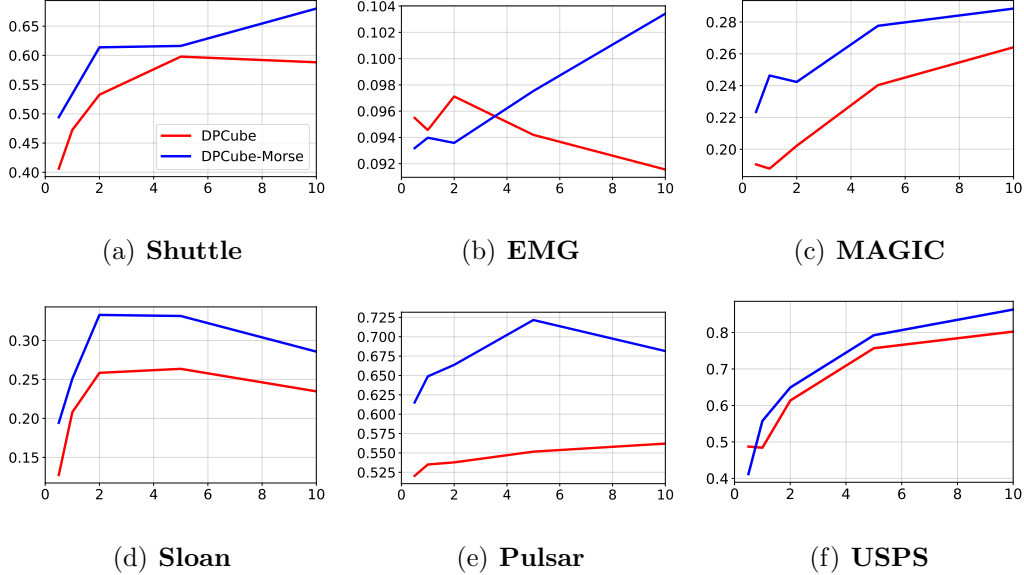


Figure 6: Clustering results of **DPCube** and **DPCube-Morse** for real-world datasets. The x-axis indicates the privacy budget ϵ , and the y-axis indicates the ARI score.

due to the small scale of the y-axis. Compared to the results in Figure 5, two main differences are observed. Firstly, for the **Shuttle** and **Pulsar** datasets, **DPCube** exhibits superior clustering outcomes in high-privacy regions compared to **DPLloyd**, and this trend is preserved for **DPCube-Morse** relative to **DPLloyd-Morse**. This underscores the versatility of the proposed method across a spectrum of baseline models, from those with lower to higher performance levels. Secondly, **DPCube** consistently outperforms **DPLloyd** for the **MAGIC** and **Sloan** datasets. For **Sloan**, **DPCube** demonstrates moderate clustering results, while **DPLloyd**'s performance diminishes. This is because **DPCube** is effective for high-dimensional data. **DPCube-Morse** also shows improved performance, significantly surpassing **DPCube**.

Figure 7 compares the clustering outcomes of **DPTree** and **DPTree-**

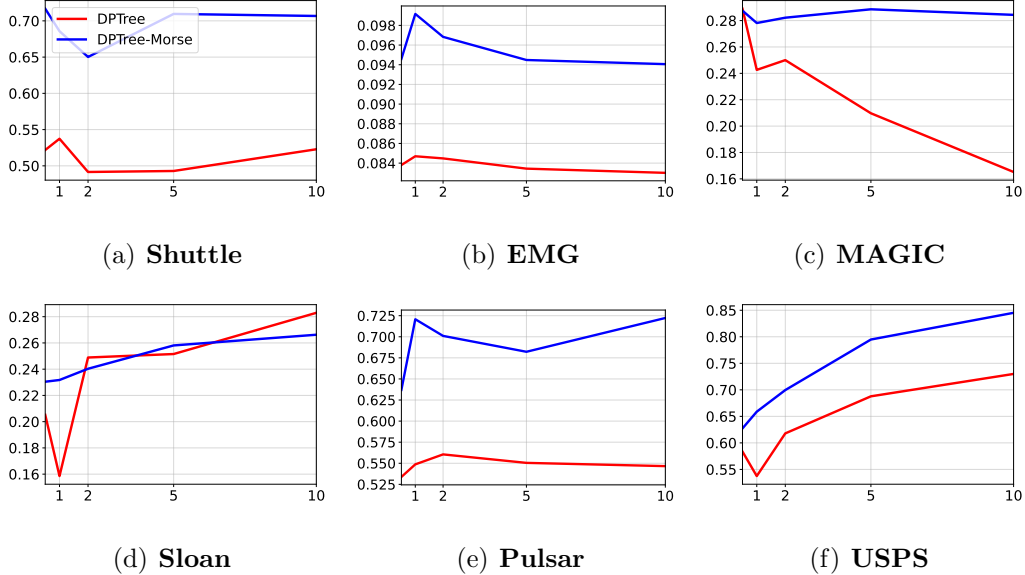


Figure 7: Clustering results of **DPTree** and **DPTree-Morse** for real-world datasets. The x-axis indicates the privacy budget ϵ , and the y-axis indicates the ARI score.

Morse. The results parallel those of other methods, with ARI scores for **DPTree-Morse** consistently outperforming **DPTree** for all datasets except **Sloan**. In the case of **Sloan** dataset, **DPTree-Morse** exhibits superior performance in high-privacy regions, while both methods demonstrate comparable performance in low-privacy regions. An interesting observation is that, for the majority of datasets, the performance of **DPTree** appears to increase as ϵ decreases, a trend also evident in the performance of **DPTree-Morse**. This phenomenon may be attributed to the original design of **DPTree** as a model satisfying local DP, with the released code subsequently modified to conform to global DP, potentially leading to unintended outcomes.

In summary, the experimental results affirm that the proposed method consistently enhances the performance of various differentially private clus-

Table 2: ARI scores of **DPMoG-hard-Morse** with different numbers of initial sub-clusters for **Pulsar** and **Magic** datasets.

Dataset	Pulsar				Magic				
	K_0	6	10	15	20	6	10	15	20
ϵ	10	0.754277	0.754838	0.766507	0.728404	0.259386	0.250220	0.248503	0.251199
	5	0.694178	0.673453	0.659280	0.664384	0.217444	0.215024	0.209862	0.216947
	2	0.688862	0.610148	0.596477	0.576486	0.083149	0.092159	0.087595	0.096408
	1	0.561494	0.584608	0.577082	0.542264	0.040309	0.047554	0.040972	0.038205

tering methods. This enhancement is particularly pronounced when the baseline method exhibits a certain level of performance. The findings suggest the potential for the proposed method to be universally applicable, contingent upon the development of superior baseline models in future research.

6.4. Effect of increasing sub-clusters

Theoretically, the proposed method can achieve the desired number of clusters by aggregating sub-clusters, regardless of the number of Gaussian sub-clusters created. However, due to the generation of different TEVs with varying numbers of centers, the final clustering outcomes exhibit variability. Therefore, an empirical investigation was conducted to assess the consistency of the final clustering performance across different numbers of sub-clusters.

Table 2 presents the clustering results of **DPMoG-hard-Morse** with varying numbers of initial sub-clusters for the **Pulsar** and **Magic** datasets. For **Pulsar**, the observed trend indicates a tendency for clustering performance to decrease as the parameter K_0 increases. Two plausible interpretations arise from these results. Firstly, the results could be attributed to the increased number of TEVs. Alternatively, the increase in the number of

sub-clusters might reduce the number of samples belonging to each cluster, thereby amplifying the impact of noise. Conversely, the ARI scores for **Magic** does not exhibit a clear dependence on K_0 . This may be attributed to the larger sample size of **Magic** compared to **Pulsar**. The sample complexity of the proposed method should be considered for future research.

7. Discussion

We proposed an effective differentially private clustering method that leverages Morse theory to express complex, nonconvex clusters without compromising privacy. Our theoretical results demonstrate that the dynamical processing associated with MoGs is completely stable and does not introduce any additional privacy loss to existing methods. Experimental results confirm that applying Morse theory enhances clustering utility for various baseline methods at the same privacy levels. Specifically, the proposed dynamical processing is versatile and can be integrated into any existing differentially private clustering approach capable of estimating an MoG density function.

Our experiments not only highlighted the strengths of the proposed method but also identified its limitations. Firstly, the proposed dynamical processing did not achieve significant performance improvements when the baseline method’s performance was poor due to high privacy levels. Additionally, excessively increasing the number of sub-clusters can be detrimental to final performance when the sample size is insufficient. It is well known from numerous studies, including [31], that the performance of differentially private algorithms is better preserved with larger sample sizes. Future research should investigate the impact of the number of sub-clusters on final perfor-

mance and determine the optimal number of subclusters.

The proposed method can be extended to a diverse set of density functions. While the kernel density function is inherently not DP-friendly, ongoing research aims to overcome these limitations since kernel methods are essential for various unsupervised learning problems such as dimensionality reduction [32] and exemplar estimation [33]. For example, [34] avoided using support vectors in the inference step by approximating the mapping of the kernel. Finally, the proposed method could be further extended by applying it to other hierarchical clustering methods [35] using different distance measures.

References

- [1] M. Ribeiro, J. Henderson, S. Williamson, H. Vikalo, Federating recommendations using differentially private prototypes, *Pattern Recognition* 129 (2022) 108746.
- [2] P. Chatterjee, D. Das, D. B. Rawat, Digital twin for credit card fraud detection: Opportunities, challenges, and fraud detection advancements, *Future Generation Computer Systems* (2024).
- [3] A. Epasto, V. Mirrokni, S. Narayanan, P. Zhong, k -means clustering with distance-based privacy, *Advances in Neural Information Processing Systems* 36 (2024).
- [4] Y. Li, X. Song, Y. Tu, M. Liu, Gapbas: Genetic algorithm-based privacy budget allocation strategy in differential privacy k -means clustering algorithm, *Computers & Security* 139 (2024) 103697.

- [5] M. Park, J. Foulds, K. Choudhary, M. Welling, Dp-em: Differentially private expectation maximization, in: Artificial Intelligence and Statistics, PMLR, 2017, pp. 896–904.
- [6] Q. Li, J. S. Gundersen, K. Tjell, R. Wisniewski, M. G. Christensen, Privacy-preserving distributed expectation maximization for gaussian mixture model using subspace perturbation, in: ICASSP 2022-2022 IEEE International Conference on Acoustics, Speech and Signal Processing (ICASSP), IEEE, 2022, pp. 4263–4267.
- [7] M. Afzali, H. Ashtiani, C. Liaw, Mixtures of gaussians are privately learnable with a polynomial number of samples, in: International Conference on Algorithmic Learning Theory, PMLR, 2024, pp. 47–73.
- [8] F. Strazzeri, R. J. Sánchez-García, Possibility results for graph clustering: A novel consistency axiom, Pattern Recognition 128 (2022) 108687.
- [9] K. Pandey, T. Bin Masood, S. Singh, I. Hotz, V. Natarajan, T. G. Murthy, Morse theory-based segmentation and fabric quantification of granular materials, Granular Matter 24 (2022) 1–20.
- [10] D. Lee, J. Lee, Dynamic dissimilarity measure for support-based clustering, IEEE Transactions on Knowledge and Data Engineering 22 (6) (2009) 900–905.
- [11] E. Cohen, H. Kaplan, Y. Mansour, U. Stemmer, E. Tsfadia, Differentially-private clustering of easy instances, in: International Conference on Machine Learning, PMLR, 2021, pp. 2049–2059.

- [12] G. Kamath, A. Mouzakis, V. Singhal, New lower bounds for private estimation and a generalized fingerprinting lemma, *Advances in neural information processing systems* 35 (2022) 24405–24418.
- [13] L. Ni, C. Li, X. Wang, H. Jiang, J. Yu, Dp-mcdbscan: Differential privacy preserving multi-core dbscan clustering for network user data, *IEEE Access* 6 (2018) 21053–21063.
- [14] F. Wu, M. Du, Q. Zhi, Density-based clustering with differential privacy, *Information Sciences* (2024) 121211.
- [15] C. Dwork, A. Roth, The algorithmic foundations of differential privacy., *Found. Trends Theor. Comput. Sci.* 9 (3-4) (2014) 211–407.
- [16] M. Bun, T. Steinke, Concentrated differential privacy: Simplifications, extensions, and lower bounds, in: *Theory of Cryptography Conference*, Springer, 2016, pp. 635–658.
- [17] M. W. Hirsch, *Differential topology*, Vol. 33, Springer Science & Business Media, 2012.
- [18] R. Palais, S. Smale, A generalized morse theory, in: *The Collected Papers of Stephen Smale: Volume 2*, 2000, pp. 503–510.
- [19] T. O. Rot, R. Vandervorst, Morse–conley–floer homology, *Journal of Topology and Analysis* 6 (03) (2014) 305–338.
- [20] J. Guckenheimer, P. Holmes, *Nonlinear oscillations, dynamical systems, and bifurcations of vector fields*, Vol. 42, Springer Science & Business Media, 2013.

- [21] H. K. Khalil, Nonlinear systems third edition, Patience Hall 115 (2002).
- [22] J. Lee, H.-D. Chiang, A dynamical trajectory-based methodology for systematically computing multiple optimal solutions of general nonlinear programming problems, *IEEE Transactions on Automatic Control* 49 (6) (2004) 888–899.
- [23] A. Samé, C. Ambroise, G. Govaert, An online classification em algorithm based on the mixture model, *Statistics and Computing* 17 (3) (2007) 209–218.
- [24] C. Hu, J. Liu, H. Xia, S. Deng, J. Yu, A lightweight mutual privacy preserving k -means clustering in industrial iot, *IEEE Transactions on Network Science and Engineering* (2023).
- [25] J. Lee, D. Lee, Dynamic characterization of cluster structures for robust and inductive support vector clustering, *IEEE Transactions on Pattern Analysis and Machine Intelligence* 28 (11) (2006) 1869–1874.
- [26] D. Lee, J. Lee, Y.-G. Yoon, A quadratic string adapted barrier exploring method for locating transition states, *Computer physics communications* 177 (1-2) (2007) 218–218.
- [27] D. Dua, C. Graff, UCI machine learning repository (2017).
URL <http://archive.ics.uci.edu/ml>
- [28] D. Su, J. Cao, N. Li, E. Bertino, M. Lyu, H. Jin, Differentially private k -means clustering and a hybrid approach to private optimization, *ACM Transactions on Privacy and Security (TOPS)* 20 (4) (2017) 1–33.

- [29] M.-F. Balcan, T. Dick, Y. Liang, W. Mou, H. Zhang, Differentially private clustering in high-dimensional euclidean spaces, in: International Conference on Machine Learning, PMLR, 2017, pp. 322–331.
- [30] A. Chang, B. Ghazi, R. Kumar, P. Manurangsi, Locally private k-means in one round, in: International Conference on Machine Learning, PMLR, 2021, pp. 1441–1451.
- [31] K. Chaudhuri, C. Monteleoni, A. D. Sarwate, Differentially private empirical risk minimization., *Journal of Machine Learning Research* 12 (3) (2011).
- [32] K. Kim, J. Lee, Sentiment visualization and classification via semi-supervised nonlinear dimensionality reduction, *Pattern Recognition* 47 (2) (2014) 758–768.
- [33] Y. Son, S. Lee, S. Park, J. Lee, Learning representative exemplars using one-class gaussian process regression, *Pattern Recognition* 74 (2018) 185–197.
- [34] J. Park, Y. Choi, J. Byun, J. Lee, S. Park, Efficient differentially private kernel support vector classifier for multi-class classification, *Information Sciences* 619 (2023) 889–907.
- [35] W.-B. Xie, Z. Liu, D. Das, B. Chen, J. Srivastava, Scalable clustering by aggregating representatives in hierarchical groups, *Pattern Recognition* 136 (2023) 109230.